doi:10.1016/j.jmb.2009.05.081 J. Mol. Biol. (2009) 391, 327–340

JMB

Available online at www.sciencedirect.com

ScienceDirect

ELSEVIER

Ligand Binding and Substrate Discrimination by UDP-Galactopyranose Mutase

Todd D. Gruber[1], M. Jack Borrok[1], William M. Westler[2], Katrina T. Forest[3]* and Laura L. Kiessling[1,4]*

[1]*Department of Biochemistry, University of Wisconsin-Madison, 433 Babcock Drive, Madison, WI 53706-1544, USA*

[2]*National Magnetic Resonance Facility at Madison, University of Wisconsin-Madison, 433 Babcock Drive, Madison, WI 53706-1544, USA*

[3]*Department of Bacteriology, University of Wisconsin-Madison, 1550 Linden Drive, Madison, WI 53706, USA*

[4]*Department of Chemistry, University of Wisconsin-Madison, 1101 University Avenue, Madison, WI 53706-1322, USA*

Received 10 March 2009; received in revised form 20 May 2009; accepted 27 May 2009
Available online 3 June 2009

Galactofuranose (Gal*f*) residues are present in cell wall glycoconjugates of numerous pathogenic microbes. Uridine 5′-diphosphate (UDP) Gal*f*, the biosynthetic precursor of Gal*f*-containing glycoconjugates, is produced from UDP-galactopyranose (UDP-Gal*p*) by the flavoenzyme UDP-galactopyranose mutase (UGM). The gene encoding UGM (*glf*) is essential for the viability of pathogens, including *Mycobacterium tuberculosis*, and this finding underscores the need to understand how UGM functions. Considerable effort has been devoted to elucidating the catalytic mechanism of UGM, but progress has been hindered by a lack of structural data for an enzyme–substrate complex. Such data could reveal not only substrate binding interactions but how UGM can act preferentially on two very different substrates, UDP-Gal*p* and UDP-Gal*f*, yet avoid other structurally related UDP sugars present in the cell. Herein, we describe the first structure of a UGM–ligand complex, which provides insight into the catalytic mechanism and molecular basis for substrate selectivity. The structure of UGM from *Klebsiella pneumoniae* bound to the substrate analog UDP-glucose (UDP-Glc) was solved by X-ray crystallographic methods and refined to 2.5 Å resolution. The ligand is proximal to the cofactor, a finding that is consistent with a proposed mechanism in which the reduced flavin engages in covalent catalysis. Despite this proximity, the glucose ring of the substrate analog is positioned such that it disfavors covalent catalysis. This orientation is consistent with data indicating that UDP-Glc is not a substrate for UGM. The relative binding orientations of UDP-Gal*p* and UDP-Glc were compared using saturation transfer difference NMR. The results indicate that the uridine moiety occupies a similar location in both ligand complexes, and this relevant binding mode is defined by our structural data. In contrast, the orientations of the glucose and galactose sugar moieties differ. To understand the consequences of these differences, we derived a model for the productive UGM–substrate complex that highlights interactions that can contribute to catalysis and substrate discrimination.

Keywords: UDP-galactopyranose mutase; *glf*; cell wall biosynthesis; mycobacteria; galactofuranose

Edited by I. Wilson

**Corresponding authors.*

Present address: L. L. Kiessling, Department of Biochemistry, University of Wisconsin-Madison, 433 Babcock Drive, Madison, WI 53706-1544, USA. E-mail address: kiesling@chem.wisc.edu.

Present address: K. T. Forest, Department of Bacteriology, University of Wisconsin-Madison, 1550 Linden Drive, Madison, WI 53706, USA. E-mail address: forest@bact.wisc.edu.

Present address: M. J. Borrok, Department of Chemical Engineering, University of Texas-Austin, Austin, TX 78712, USA.

Abbreviations used: FP, fluorescence polarization; Gal*f*, galactofuranose; UDP, uridine 5′-diphosphate; UDP-Gal*p*, UDP-galactopyranose; UGM, UDP-galactopyranose mutase; UDP-Glc, UDP-glucose; FAD, flavin adenine dinucleotide; STD, saturation transfer difference; UDP-Glc*p*, UDP-glucopyranose; PDB, Protein Data Bank; UMP, uridine 5′-monophosphate; UDP-Fl, UDP-fluorescein; NIH, National Institutes of Health.

Introduction

Galactofuranose (Gal*f*) residues are cell wall components of numerous microorganisms, including pathogenic strains of *Klebsiella pneumoniae* and *Escherichia coli*, as well as mycobacterial species.[1–6] The furanose form of galactose is also present in eukaryotic pathogens such as *Leishmania major*, *Aspergillus fumigatus*, and *Trypanosoma cruzi*.[7–9] The presence of Gal*f* in many disease-causing organisms provides an impetus to understanding the mechanisms underlying its incorporation. The biosynthetic precursor of Gal*f*-containing glycoconjugates is uridine 5c-diphosphate (UDP) Gal*f*, which is generated by the enzyme UDP-galactopyranose mutase (UGM). The gene encoding UGM (*glf*) is essential for viability in mycobacteria.[10] UGM is also vital in eukaryotes, as strains of *Aspergillus* spp. lacking the enzyme show defects in growth,[11] cell wall biosynthesis,[12] and virulence.[13] Similarly, deletion of the gene encoding UGM in *L. major* results in attenuated virulence.[14] Because there is no human homolog of UGM,[15] it has been suggested that this enzyme can serve as a target of antimicrobial agents, especially antimycobacterial agents.[16–19] Intriguingly, UGM inhibitors that block mycobacterial growth have been synthesized.[19] These promising developments provide an incentive to extend the current understanding of UGM catalysis.

UGM is a flavoenzyme that catalyzes the interconversion of UDP-galactopyranose (UDP-Gal*p*) and UDP-Gal*f* (Fig. 1a).[3] Mechanistic studies suggest that its noncovalently associated flavin adenine dinucleotide (FAD) plays an important role in catalysis.[22] Specifically, UGM is active only when the cofactor is reduced.[22] The reduced flavin has been suggested to have several different functions, from mediating transient electron transfer (single electron transfer or hydride transfer) to serving a structural role within the protein scaffold.[5,21,23,24] We provided evidence for the intermediacy of a flavin–galactose iminium adduct (Fig. 1b).[20,25] In this mechanism, the N5 of reduced flavin acts as a nucleophile (S_N1 or S_N2 attack) to generate a covalent flavin–galactose adduct.[20,25] A radical mechanism that also affords the iminium intermediate was subsequently put forth,[26,27] but complications regarding this proposal have not yet been

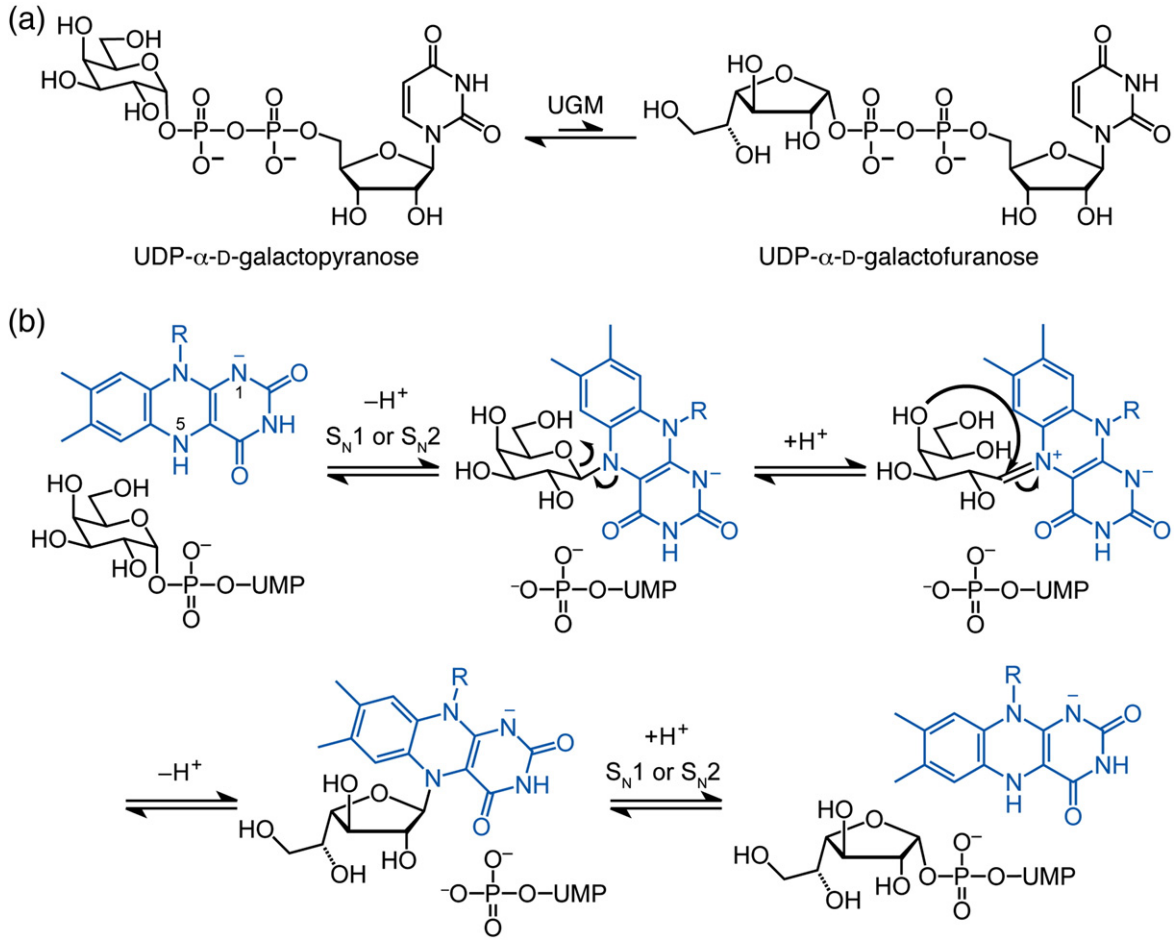

Fig. 1. Interconversion of UDP-Gal*p* and UDP-Gal*f* catalyzed by UGM. (a) The reaction catalyzed by UGM. (b) Nucleophilic mechanism for catalysis by UGM; the reaction could proceed by either S_N1 or S_N2, as described previously.[20] N1 is depicted as negatively charged, as reported previously.[21]

addressed.[28] The hypothesis that a flavin-derived iminium ion mediates catalysis via a previously unknown mechanistic pathway provides an incentive to determine the mode of substrate binding.

Because the structure of a substrate or substrate analog bound to UGM has been elusive, X-ray crystallography has provided valuable but incomplete information. The first structure (of *E. coli* UGM) revealed that the enzyme is a dimer in which each subunit harbors a FAD cofactor.[22] The cofactor sits in a cleft lined with highly conserved residues. Structures of UGM homologs from *Mycobacterium tuberculosis* and *K. pneumoniae* corroborate these findings.[29] Complementary results have been obtained from studying the UGM from *K. pneumoniae* using site-directed mutagenesis. When the importance of highly conserved residues was evaluated,[22,30] two Arg residues were found to be essential for catalysis.[30] The identification of one of these, Arg174, was unexpected because the available crystallographic data place this residue outside the putative active site. This residue is located on a mobile loop adjacent to the putative active site pointing away from the flavin.[22,29] Molecular dynamics simulations suggest that this loop closes upon substrate binding, thereby orienting the Arg174 side chain toward the pyrophosphoryl group of the ligand.[30–32] Thus, several lines of evidence indicate that UGM undergoes a conformational change upon ligand binding, and we set out to explore this issue.

We envisioned using X-ray crystallographic analysis to address directly how UGM binds its substrate. Because UDP-glucose (UDP-Glc) differs from the substrate UDP-Gal*p* only by an equatorial rather than axial C4-OH group, we reasoned that UDP-Glc would not undergo reaction but rather serve as an unreactive substrate analog. Indeed, we were able to crystallize the complex and to determine its structure. The resulting structure of the complex defines the location of the active site and reveals how conserved amino acids interact with the uridine diphosphoryl portion of the ligand.

Consistent with the proposal that the reaction proceeds through a flavin–galactose adduct, the sugar residue of the substrate analog is in the vicinity of the flavin. Despite its similarity to the natural substrate, however, UDP-Glc does not give rise to the spectroscopic signal indicative of the putative flavin iminium ion.[20,33] This observation highlights the difference between the reactivity of UDP-Glc and the reactivity of the substrate UDP-Galp. It is also consistent with the orientation of UDP-Glc in the complex, which precludes bond formation with the reduced flavin. The data indicate that the equatorial C4-OH group of UDP-Glc influences the structure of the complex and thereby renders the iminium adduct inaccessible. These findings provide a structural rationale as to why UDP-Glc, which is present in significant concentrations in the cell, does not interfere with the recognition of substrate by UGM.

Results

UDP-Glc functions as a UGM ligand

The structural similarity of UDP-Glc and UDP-Gal*p* led us to postulate that the former could illuminate how UGM binds its substrate. We assessed the ability of UDP-Glc to bind UGM by comparing the affinities of UDP-Gal*p* and UDP-Glc for oxidized and reduced UGM. For oxidized UGM, we utilized a binding assay in which a ligand of interest competes with a UDP-linked fluorescein probe.[17] The application of this approach yielded a K_d value of 290±40 μM for the complex of UDP-Gal*p* and oxidized UGM, similar to that determined using a Trp fluorescence assay (220 μM).[32] This value is 5- to 6-fold higher than that reported for the reduced enzyme complex (52 μM[27] and 66 μM[32]), a preference similar to that observed previously in saturation transfer difference (STD) NMR experiments.[31,34] The natural substrate UDP-Gal*p* therefore

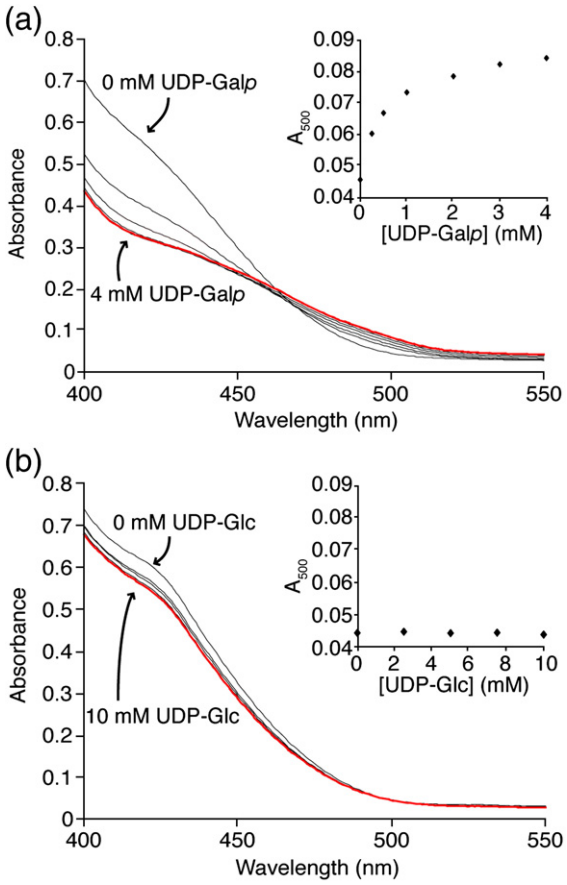

Fig. 2. Spectrophotometric studies probing for a flavin-derived iminium ion. Spectra were recorded as 0–4 mM UDP-Gal*p* (a), or 0–10 mM UDP-Glc (b) was titrated into a sample of reduced UGM. The red line represents the absorbance spectrum at the highest concentration of the ligand. Inset: Absorbance at 500 nm, the wavelength of iminium ion absorbance. A change is detected for UDP-Gal*p*, but not for UDP-Glc. Results in (a) have been published previously[20] and are shown for comparison.

exhibits a preference for the active reduced enzyme. For comparison, we evaluated the selectivity of UDP-Glc. As with UDP-Gal*p*, UDP-Glc displaces the fluorescent UDP derivative, indicating that all three UDP derivatives bind in the same active site. The K_d value for oxidized UGM binding to UDP-Glc (550±100 μM) is only 2-fold weaker than that for UDP-Gal*p*. The UDP-Glc bound to the reduced enzyme with a K_d value of 750±250 μM. Thus, the oxidized UGM shows only a subtle (2-fold) penchant for binding UDP-Gal*p* over UDP-Glc, but the reduced form exhibits a preference of over 10-fold. Despite the preference for binding UDP-Gal*p*, the affinity data indicate that UDP-Glc can serve as a ligand for UGM.

UDP-Glc is not a substrate for UGM

Given the similarity of UDP-Glc and UDP-Gal*p*, we wanted to confirm that UDP-Glc was not a substrate for UGM. For the structural analysis of an enzyme–ligand complex, it is desirable that a stable complex be formed. The configuration of the C4 hydroxyl group of UDP-Glc (equatorial) relative to that of UDP-Gal*p* (axial) should preclude the catalytic conversion of UDP-glucopyranose (UDP-Glcp) into the highly thermodynamically disfavored glucofuranose form.[35] As expected, we detected no UGM-catalyzed conversion of UDP-Glcp into UDP-glucofuranose. It is plausible, however, that UDP-Glc could give rise to the spectroscopic signature attributed to the flavin–iminium intermediate (Fig. 1b).[33] Previously, we demonstrated that when UDP-Gal*p* and reduced UGM are mixed, an increase in absorbance at 500 nm is observed.[20] We therefore tested whether exposure of UGM to UDP-Glc would afford a similar result. No change was detected (Fig. 2). These data suggest that despite the structural similarity between UDP-Glc and UDP-Gal*p*, UGM discriminates against the former not only at the level of binding but also in catalysis. Moreover, these results indicate that UDP-Glc can serve as a stable substrate analog for structural studies of UGM.

Structure of UGM complexes

Previous attempts to obtain the structure of a complex between UGM and its substrate UDP-Gal*p* were unsuccessful.[22,29] We therefore conducted crystallization trials in the presence of the substrate analog UDP-Glc. From a solution containing 5 mM UDP-Glc, crystals were obtained. The structure of UGM bound to UDP-Glc was solved by molecular replacement and refined against 2.5 Å resolution data (Table 1). The final structure exhibits excellent geometry, with 98.4% of residues in favorable Ramachandran orientations.[36] The asymmetric unit contains an entire UGM dimer (Fig. 3a), but each subunit adopts a different conformation. Monomer A represents a fully liganded, closed conformation, whereas monomer B represents a partially liganded, open conformation.

The flavin cofactor is in the active site

Despite the conformational differences between the two monomers, the ligand is adjacent to the flavin in both. Because the substrate analog is more well defined in closed monomer A, our analysis focuses on this monomer. UDP-Glc is bound such that its glucose residue is near the isoalloxazine ring of flavin (Fig. 3b); the minimum flavin–glucose distance is only 2.9 Å. The proximity of the flavin and the sugar residue of the substrate analog is consistent with the putative mechanism involving covalent catalysis.[20,25] The UDP portion of the ligand makes close contacts with the remainder of the highly conserved binding pocket (see the text below). In addition, the side chain of Arg174, which points away from the active site in unliganded structures, is located in the active site in the complex (Fig. 4). The guanidinium moiety of Arg174 is oriented in a manner consistent with its predicted role in binding the pyrophosphoryl group of the substrate.[30–32]

Monomer comparison

The differences in monomers A and B provide insight into the conformational changes that can

Table 1. Data collection and refinement statistics

Data collection	
Resolution limits (Å) (last shell)	50.0–2.45 (2.54–2.45)
Unique reflections (*n*)	41,161 (4042)
Completeness (%)	98.6 (97.0)
R_{sym}[a] (%)	11.0 (36.6)
$I/(\sigma I)$	14.8 (4.2)
Redundancy	4.9 (4.9)
Wilson *B*-factor (Å^2)	53.9
Space group	$P4_1$
Unit cell parameters *a*/*b*/*c* (Å)	94.0/94.0/130.3
Refinement statistics	
Resolution range (Å)	30.0–2.45 (2.51–2.45)
R_{cryst}[b] (%)/R_{free}[c] (%)	19.2 (25.6)/23.8 (32.1)
Protein atoms	6240
Water molecules	195
Hetero atoms	163
Isotropic average temperature factors (Å^2)	
Overall	45.8
Protein	45.9
Water	43.4
FAD (monomer A)	39.3
FAD (monomer B)	37.6
UDP-Glc	59.7
UMP	61.4
Estimated coordinate error from Luzzati plot (Å)	0.25
RMSD from ideal	
Bond length (Å)	0.018
Bond angle (°)	1.7
Ramachandran plot (% favored/% allowed)[36]	98.4/100.0

[a] $R_{sym}(I) = \sum_{hkl}\sum_i | I_i(hkl) - \langle I(hkl)\rangle | / \sum_{hkl}\sum_i I_i(hkl)$, where $I(i)$ is the intensity of the *i*th observation of the *hkl* reflection, and $\langle I(hkl)\rangle$ is the mean intensity from multiple measurements of the *h*,*k*,*l* reflection.

[b] $R_{cryst}(F) = \sum_{hkl} | F_{obs}(hkl) - F_{calc}(hkl) | / \sum_{hkl} F_{obs}(hkl)$, where $F_{obs}(hkl)$ and $F_{calc}(hkl)$ are the observed and calculated structure factor amplitudes for the *h*,*k*,*l* reflection, respectively.

[c] R_{free} is R_{cryst} calculated for a randomly selected test set of reflections (5%) not included in the refinement.

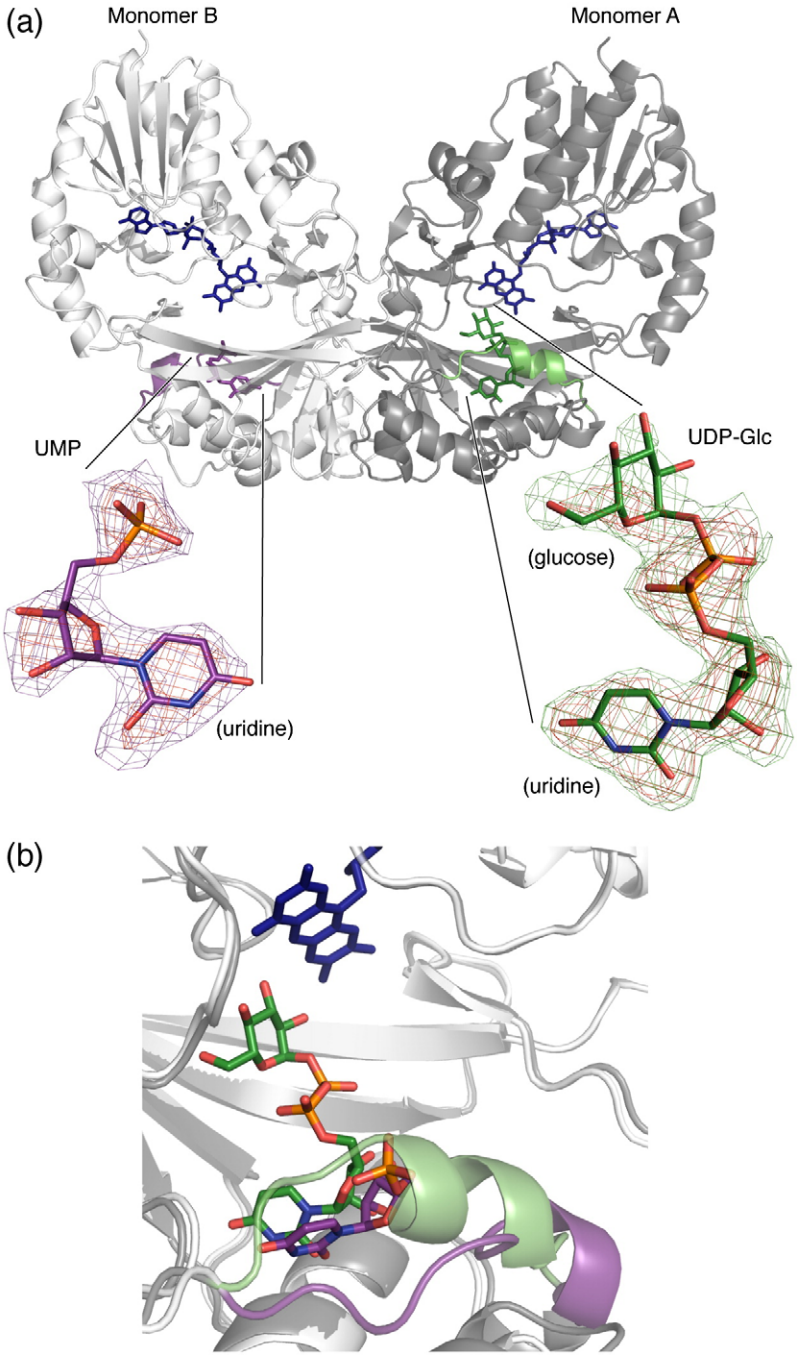

Fig. 3. The structure of the UGM–UDP-Glc complex reveals ligand orientation in the UGM active site. (a) View of the UGM dimer. FAD (blue), UDP-Glc (green), monomer A mobile loop (green), UMP (purple), monomer B mobile loop (purple). UMP inset: Omit map showing difference density ($F_o - F_c$) for UMP in monomer B. The red grid is contoured at 4σ, and the purple grid is contoured at 2.5σ (C, purple; O, red; N, blue; P, orange). UDP-Glc inset: Omit map showing difference density ($F_o - F_c$) for UDP-Glc in monomer A. The red grid is contoured at 4σ, and the green grid is contoured at 2.5σ (C, green). (b) Overlay of monomers A and B depicting mobile loop (residues 167–177) and ligand orientation. Closed monomer A loop and carbons are shown in green, whereas open monomer B loop and carbons are shown in purple. Residues 125–166 also move significantly (up to 6 Å C^{α} movement) to accommodate mobile loop restructuring (data not shown).

occur upon ligand binding. Superposition of the monomers results in a C^{α} root-mean-square deviation (rmsd) of 1.45 Å. When the same operation is performed using monomer A and the unliganded *K. pneumoniae* UGM monomer [Protein Data Bank (PDB) code 2BI7],[29] an rmsd of 1.41 Å is obtained. In contrast, a comparison of monomer B with *K. pneumoniae* UGM yields a significantly smaller rmsd of 0.88 Å. The major difference between monomers A and B is observed in residues 125–177. When this region is excluded from the calculation (i.e., residues 2–124 and 178–384 were superimposed), an rmsd of 0.86 Å results. Together, the results indicate that monomer B adopts a conformation similar to that

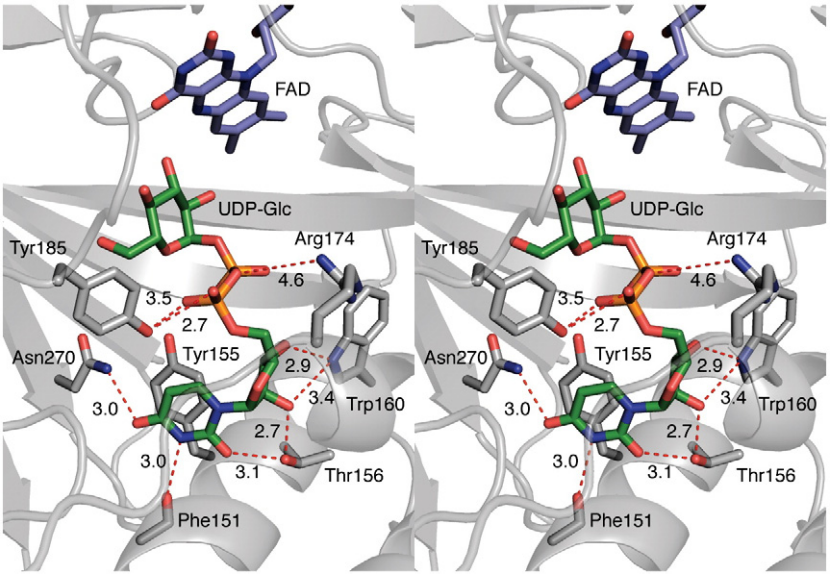

Fig. 4. Stereo view of contacts between the uridine moiety of UDP-Glc and protein atoms in monomer A. The nucleoside portion of UDP-Glc interacts with conserved amino acids (C, gray; other atoms colored as described above) such as Trp160, as seen through the semitransparent mobile loop. The stacking distance between Tyr155 and uracil is approximately 3.5 Å.

observed previously in structures of unliganded UGM homologs, whereas monomer A represents a closed form.

In the open monomer B, the active site is highly solvent exposed, and a clear pattern of electron density is obtained only for the uridine 5′-monophosphate (UMP) portion of the ligand (Fig. 3a). In contrast, the entire ligand in closed monomer A is well ordered (Fig. 3a). The positions of the uridine moieties are similar in both (Fig. 3b), but those of the α-phosphoryl groups are not (they differ by 6 Å). In the more open monomer B, the α-phosphoryl group is located toward the active-site opening, while in monomer A, it is oriented toward the FAD cofactor.

Ligand binding induces conformational change

A major difference between monomers A and B is the conformation of the mobile loop.[29,30] In monomer A, these residues (residues 167–177), which are adjacent to the uridine diphosphoryl portion of the ligand, close over the active site (Fig. 3b). This conformational change involves extending a short helix composed of residues 169–171 to encompass residues 172–174. In unliganded structures,[22,29] this loop adopts a variety of conformations. Only in the *K. pneumoniae* structure[29] does this loop exhibit any secondary structure; residues 169–172 constitute a short helix. In monomer A, loop closure and helix formation result in the movement of Arg174 to within 4.6 Å of the ligand pyrophosphoryl group. Arg174 has high *B*-values and gives rise to a relatively weak electron density, yet its ability to occupy a position near the pyrophosphoryl moiety is notable. This movement toward the ligand is consistent with previous biochemical data and with a purported role for this conserved residue in phosphoryl group binding.[30–32]

Orientation of uridine nucleotide

Because complete density for UDP-Glc is observed (Fig. 3a), the monomer A structure provides insight into the contributions of highly conserved catalytic residues[22,30] to substrate binding (Fig. 4). For example, the plane of the uracil moiety of UDP-Glc is parallel with that of invariant Tyr155, and the two aromatic rings are separated by approximately 3.5 Å. Their proximity and orientation indicate that this π-stacking interaction contributes to substrate binding. This observation was unexpected, as previous models and molecular dynamics simulations incorporated π-stacking interactions between uracil and invariant Trp160.[22,29–32,34] Although Trp160 does not contribute to uracil binding, the indole nitrogen can form a bifurcated hydrogen bond to the C2-hydroxyl and C3-hydroxyl groups of the ribose ring. The uracil N3 is within hydrogen-bonding distance of the backbone carbonyl of Phe151, as are the uracil O4 and the side-chain carboxamide group of Asn270. The hydroxyl group of Thr156 is positioned to engage in hydrogen bonding both with C2-OH of ribose and with O2 of uracil. Tyr185 is located in proximity to the α-phosphoryl group. Hydrophobic residues also define parts of the uridine-binding pocket, and Phe152, Leu97, and Leu175 all are within van der Waals distance (3.1–3.5 Å) of the ligand.

Orientation of glucose residue

In the closed conformation, the glucose residue of UDP-Glc is adjacent to the flavin. Proximity is

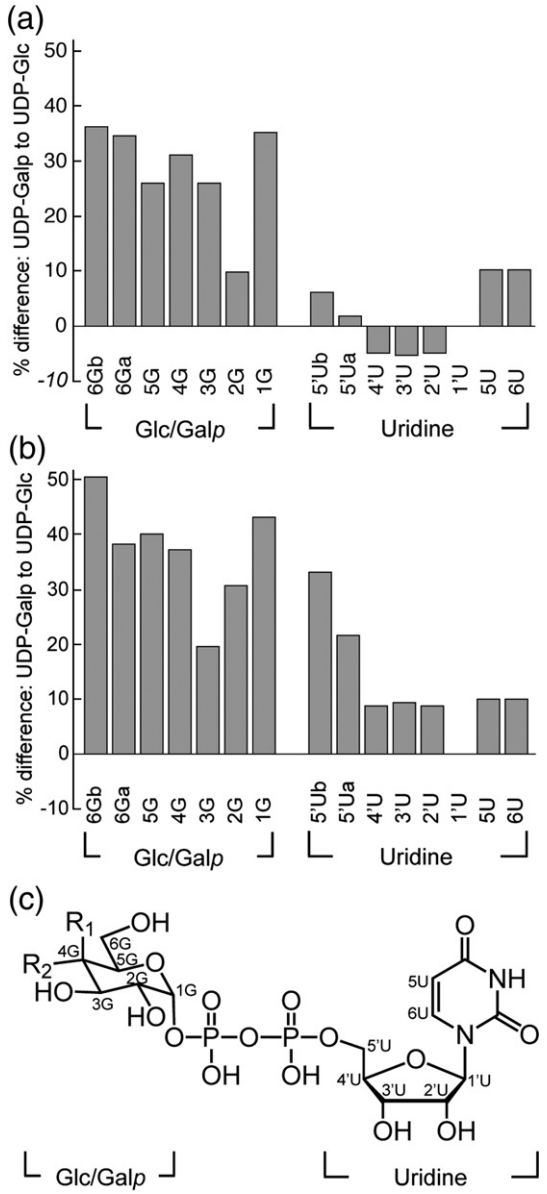

Fig. 5. Analysis of the binding of UDP-Gal*p* and UDP-Glc to UGM using STD-NMR. Percent differences between UDP-Glc and UDP-Gal*p* STD-NMR intensities in oxidized UGM (a) and reduced UGM (b) are charted by atom. All STD intensities were normalized to proton 1′U at 100%. Percent differences represent the difference between UDP-Gal*p* and UDP-Glc STD intensities, divided by UDP-Gal*p* STD intensities. Results from one representative experiment are shown. U = uridine; G = glucose or galactose. (c) Structure of UDP-Glc/UDP-Gal*p*. UDP-Glc: R_1 = H; R_2 = OH. UDP-Gal*p*: R_1 = OH; R_2 = H. Repetition of the experiment afforded similar results (Supplementary Fig. 1).

required for the putative covalent catalysis mechanism in which a bond is formed between the flavin N5 and the anomeric position of the sugar (Fig. 1b). In monomer A, however, 6.0 Å separates these nucleophilic (flavin N5) and electrophilic (sugar C1) groups. In addition, the UDP leaving group[23] is not oriented favorably for a substitution reaction (S_N1 or S_N2). The relative positions of the UDP-Glc and the flavin are consistent with the observation that no signal indicative of a flavin-derived iminium ion is detected upon the addition of UDP-Glc (Fig. 2). These differences led us to hypothesize that the orientation of the glucose moiety in the complex does not mirror that of the Gal*p* moiety.

STD-NMR reveals that uridine components of UDP-Glc and UDP-Gal*p* bind similarly

To compare the UDP-Glc and UDP-Gal*p* binding modes, we employed STD-NMR spectroscopy. In this method, protein resonances are saturated with a radiofrequency pulse, and magnetization is transferred to proximal ligand protons.[37] The efficiency of transfer depends upon the relative proximity and orientation of the ligand and protein protons. STD values thus reflect binding interactions; therefore, a comparison of the STD values obtained for related ligands can report on their relative binding orientations. Others have used STD-NMR to investigate UGM, and these studies have indicated that UDP-Gal*p* binds more tightly to reduced UGM than does UDP.[31,34] Given this successful application of STD-NMR in monitoring ligand binding to UGM, we employed it to compare the binding of UDP-Glc and UDP-Gal*p* under both oxidizing (catalytically inactive) and reducing (active) conditions. When UGM is oxidized (Fig. 5a), the uridine STD signals of both UDP-Glc and UDP-Gal*p* are similar, with an average difference (absolute value) of 6%. A much larger difference (28%) was observed for sugar signals from the hexose sugar moiety (Glc or Gal*p*). These results indicate that the uridine portion of each ligand binds in a similar manner but that the interactions of the sugar moieties differ. The data from the reduced complex follow a similar trend: a 15% difference for the uridine signals compared to 37% for those of the sugar portion (Fig. 5b). The larger differences for the reduced complex are consistent with our finding that this form of UGM more effectively discriminates between UDP-Glc and the substrate UDP-Gal*p*. We also observed that the largest differences in uridine signal for the reduced complex are at ribose C5, the position connected to the α-phosphoryl group. As the C5 position is likely to be most strongly influenced when the orientations of the sugar moiety vary, these data further support the conclusion that the uridine groups bind similarly but that the mode of sugar binding depends upon its identity.

Energy-minimized active-site model for substrate binding

We used our X-ray structure, previous data, and the results of our comparative analysis of UDP-Glc and UDP-Gal*p* to develop a model of the complex of UGM with its substrate UDP-Gal*p*. In constructing such a model, we assumed that the binding mode of the UMP moiety in monomer A is preserved in the UDP-Gal*p* complex. We then explored whether the Gal*p* moiety could access an orientation that is consistent

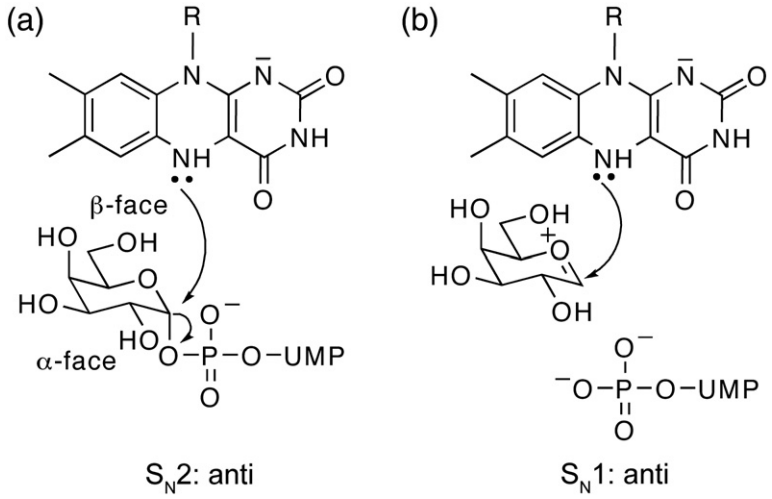

Fig. 6. Geometries consistent with nucleophilic attack. (a) An S_N2 reaction in which the N5 of reduced flavin attacks the anomeric position from the β-face of UDP-Gal*p*, causing the UDP to leave from the α-face. (b) S_N1 reaction, anti-relationship. An S_N1 reaction can proceed with UDP leaving from the α-face of UDP-Gal*p* to form an oxocarbenium intermediate. The N5 of the reduced flavin can then attack from the β-face.

with our observation that a covalent flavin–galactose adduct can form under catalytic conditions. Specifically, the preferred geometry for the production of this species entails an anti orientation of the flavin and pyrophosphoryl leaving group (Fig. 6).

To create the model, we oriented UDP-Gal*p* in the active site analogously to UDP-Glc (Fig. 7a). Rotatable bonds in the substrate were altered, such that the β-phosphoryl moiety could interact with Tyr314 in a manner similar to that observed for the α-phosphoryl moiety and Tyr185. In the resulting arrangement, an interaction between the β-phosphoryl group and Gln159 is maintained. The anomeric carbon–β-phosphoryl oxygen (glycosidic) bond was then positioned anti to the nucleophilic flavin N5. The complex was then subjected to energy minimization (see Materials and Methods). In the model that results (Fig. 7b; Supplementary Fig. 2), the distance from flavin N5 to the anomeric carbon of UDP-Gal*p* is 4.2 Å, consistent with covalent catalysis

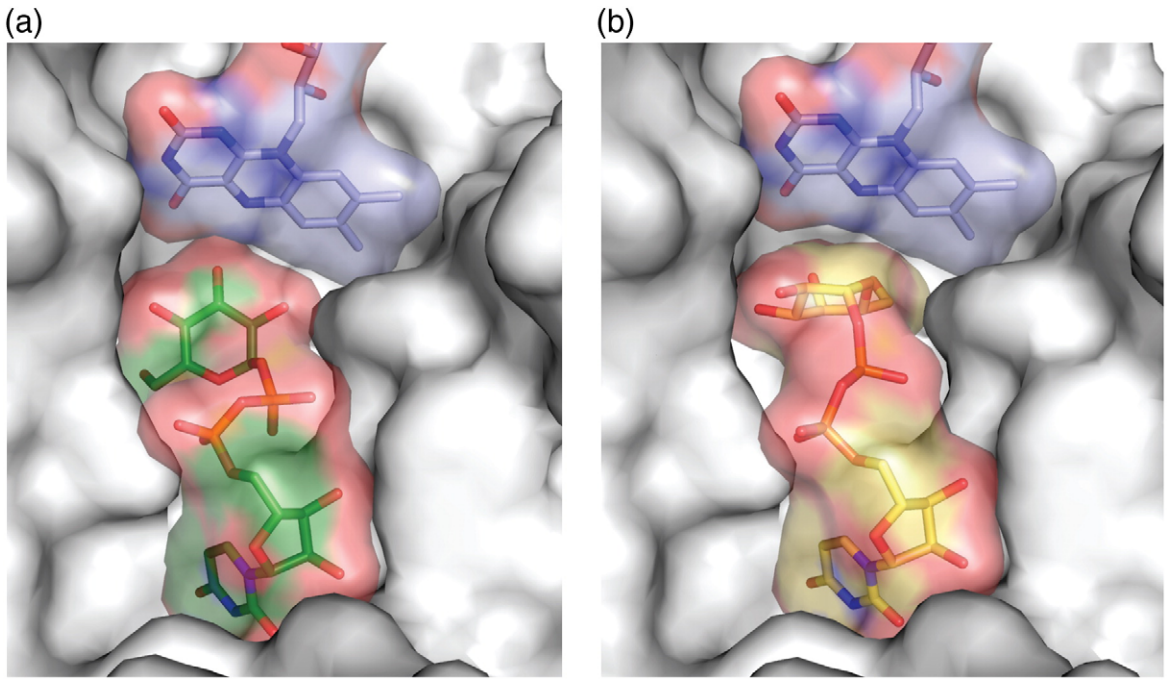

Fig. 7. The ligand-binding pocket of UGM. (a) Monomer-A-binding pocket with UDP-Glc bound. UGM is rendered as a surface to depict the binding pocket (coloring as in Fig. 3). (b) Binding pocket showing the UDP-Gal*p* model [colored as in (a), except that carbons are shown in yellow]. In (a) and (b), residues 163–177 and 340–384 were deleted for clarity.

by flavin. This distance is similar to that observed between the N5 of flavin and the anomeric carbon (C1) of the substrate, which resulted from docking studies of UDP-Gal*p*[34] and UDP-Gal*f*.[31] Still, the uridine orientation predicted by calculations is very different from that observed in our structure (UDP-Glc) and model (UDP-Gal*p*) (see Discussion).

The C4-OH of UDP-Gal*p* in the minimized model points toward the backbone carbonyl of Pro59. Intriguingly, UDP-Glc would not be able to bind to UGM in this conformation. A steric clash between the equatorial C4-OH of UDP-Glc and invariant Arg280 (~1.3 Å separation) precludes the formation of a UDP-Glc complex that is poised to form a flavin–sugar bond. This steric effect is alleviated when UDP-Glc adopts the orientation observed in monomer A. In the model of the UDP-Gal*p* complex, the β-phosphoryl group is closer to Arg280 (5.2 Å in the modeled substrate complex compared to 5.7 Å in the structure of the substrate analog). Both distances are too long for hydrogen bonding, supporting the possibility that the role of this absolutely conserved residue is not to facilitate initial substrate binding but rather to stabilize the UDP intermediate during turnover.[30,31] Alternatively, Arg280 may interact with the 6-OH of Gal*p*; the significance of this functional group to UGM catalysis has recently been investigated.[38,39] In the model, the distance separating the guanidinium group of Arg280 and the 6-OH of the Gal residue is 2.9 Å, suggesting that the guanidinium side chain serves as a hydrogen-bond donor and that 6-OH serves as an acceptor. Either proposed role for Arg280 is consistent with its position in the model. Thus, our substrate–UGM model is consistent with the findings reported herein and other data.[20,22,29,30,32]

Discussion

The substrate-binding pocket of UGM has been identified and defined by the first X-ray crystal structure of UGM with a bound ligand. Analyses of the UGM complexes of the ligand UDP-Glc and the substrate UDP-Gal*p* using STD-NMR and molecular modeling indicate that both bind in the same pocket. Thus, the active site can be identified directly, and it is adjacent to the flavin cofactor. This location is consistent with a role for flavin in catalysis. The uridine component of either the substrate or the substrate analog binds tightly in a pocket lined with conserved residues. Uridine binding orients the hexose (Gal*p* or Glc) moiety toward the flavin. A key feature of ligand binding is that it can induce a conformational change in a mobile loop that closes over the active site,[31,32,34] thereby nudging the sugar moiety and cofactor into close proximity.

Role of conserved residues in ligand binding

The structure of the complex of UDP-Glc and UGM reveals features that illuminate, expand upon, and refute ideas inferred from previous models. For example, our results reveal an unexpected role for conserved Trp160. Previous mutagenesis experiments indicate that the activity for the Trp160Ala variant is decreased by 6 orders of magnitude.[30] To account for this dramatic decrease, we conducted docking studies suggesting that the uracil ring of the substrate stacks upon Trp160.[22,29–31,34] This orientation also was invoked in a study in which it was postulated that the substrate bridges the Trp160 and flavin sites.[32] Our crystallographic structure refinement of the UDP-Glc complex indicates a very different role for Trp160. It engages in an unusual tryptophan–ribose interaction in which it interacts with the C2-OH and C3-OH of the ribose residue (Fig. 4). Additionally, we have found that the uracil ring does indeed engage in a stacking interaction, but not with Trp160; rather, it interacts with Tyr155, an absolutely conserved active-site residue. Phenylalanine substitution of this residue results in a significant decrease in substrate binding affinity (K_m value diminished by 15-fold).[30] Our finding that Tyr155 participates in a stacking interaction provides a rationale for this decrease. It remains unclear, however, whether this decrease in affinity is due to a fundamental difference in the stacking ability of tyrosine and phenylalanine[40] or to a misalignment of residues due to loss of hydrogen bonding from the tyrosine phenol. Whatever the source of the affinity difference between wild-type UGM and the Tyr155Phe variant, uracil–tyrosine stacking interactions similar to those we have observed are found commonly in RNA-binding proteins.[41]

In addition to providing insight into the importance of Tyr155 and Trp160, our structure reveals the function of three other highly conserved active-site aromatic residues: Tyr185, Tyr314, and Tyr349. These residues have been shown to be important for catalysis[22,30] and have been implicated in hydrogen-bonding[22] or aromatic interactions.[30] Of these five aromatic residues, only Tyr155 clearly engages in π-stacking in the UDP-Glc complex. It is possible, however, that Tyr349 also engages in a cation–π interaction (Supplementary Fig. 2).[42] It could stabilize a positive charge (full or partial) that develops at the anomeric position of galactose in the transition state of a substitution reaction (either S_N1 or S_N2). Another potential role for Tyr349 is to use hydrogen bonding to facilitate an orientation of Gal*p* that allows for bond formation between the reduced flavin and Gal*p*. The remaining three conserved aromatic residues of the active site, Trp160, Tyr185, and Tyr314, utilize hydrogen bonding to interact with the ligand. For instance, Tyr185 is poised to interact with the α-phosphoryl group of UDP-Glc. The model of the substrate complex suggests that Tyr314 contacts the β-phosphoryl group through a similar mode of interaction. In addition to their role in hydrogen bonding, the aromatic character of these three residues may serve to stabilize substrate binding. It is interesting to note that the carbohydrate

binding sites of lectins often are lined with aromatic residues.[43–45]

A comparison of positions that differ between prokaryotic and eukaryotic UGMs suggests conservation of function. For example, the aforementioned Tyr185, which is conserved in prokaryotes, corresponds to Trp in eukaryotic UGMs.[30,46] The indole NH, like the phenol of Tyr185, could serve as a hydrogen-bond donor to the α-phosphoryl group (Supplementary Fig. 3). Similarly, another residue that is highly conserved in prokaryotes, Thr156, is in position to engage in hydrogen bonding to both uracil (O2) and ribose (C2-OH). In eukaryotes, however, an asparagine is typically found at this position.[30,46,47] Like threonine, asparagine could engage in hydrogen bonding with two sites on the ligand. Asn270 is another conserved residue in prokaryotes that differs from the corresponding tyrosine residue in eukaryotes; however, both can form a hydrogen bond with uracil (O4). Although many side-chain variations can be rationalized, some differences between the conserved positions in prokaryotes *versus* eukaryotes are not readily understood. The prokaryotic residue Gln159, which is in position to bind the β-phosphoryl group, is commonly a valine in eukaryotes. The basis for this preference awaits a structure of a eukaryotic UGM.

Conformational changes and loop movement

Our structure provides snapshots of two distinct modes of substrate interaction. Open monomer B, with its partially ordered ligand, appears to represent an encounter complex in which the nucleoside is bound but the glucose moiety is disordered. Monomer A provides an alternative view in which the mobile loop is closed over the active site. We anticipate this conformation to be closer to the catalytically active form of the enzyme. The closed and open conformations observed in one dimer of UGM are reminiscent of other crystal structures showing monomer asymmetry, some of which have been consistent with known evidence for positive cooperativity[48] or extreme negative cooperativity (half-site reactivity).[49] Neither type of cooperativity has been reported for UGM. Based on inspection of crystal lattice interactions in our UGM structure, it is likely that packing interactions explain the asymmetry in this case. Monomer A participates in crystal packing that appears to stabilize the closed orientation, whereas similar interactions are lacking in open monomer B.

The differences between monomers A and B provide new information about the UGM mobile loop. Results from extensive molecular dynamics simulations have shown that loop movement in the presence of substrate allows for transient closing of the active site and reorientation of Arg174 such that it can interact with ligand phosphoryl groups.[30–32] The key changes that occur in the mobile loop during this process are now apparent. The Arg174 side chain is not reoriented by translocation of the loop alone; rather, its change in position is a consequence of the extension of the helix within the loop region. Although our results indicate that Arg174 is situated in the active site, even in closed monomer A, it is 4.6 Å from the nearest ligand phosphoryl oxygen. This distance is longer than might be expected; however, our STD-NMR data indicate that additional adjustments in the active site must occur when the natural substrate UDP-Gal*p* binds. We note that Arg174 may also stabilize the UDP leaving group, as suggested above for Arg280.[30,31]

Two additional residues, Phe152 and Leu175, also undergo significant movements as UGM goes from the unbound state to the bound state (Supplementary Fig. 3). The aromatic side chains Phe152 and Tyr155 sandwich the uracil ring of the ligand. To adopt this position, Phe152 swivels by approximately 2 Å from its location in the open monomer B or the unliganded *Klebsiella* UGM structure. During closure, Leu175 of the mobile loop translocates by approximately 8 Å from its position in the open form. In the complex, it is adjacent to the bridging oxygen of the ribose moiety and Phe152. Thus, Phe152 and Leu175 form a significant portion of the uridine binding site, and their movement contributes to the creation of shape complementarity. The significant repositioning of these residues in the bound complex underscores the difficulty of modeling the uridine binding orientation in the absence of a structure.[22,29–32,34]

Comparison between UDP-Glc and UDP-Gal*p* binding to UGM

Despite the structural similarity of UDP-Glc and UDP-Gal*p*, their interactions with UGM are quite different. Both ligands bind to the enzyme, yet UDP-Glc binds 10-fold more weakly to the catalytically active, reduced state. Moreover, its addition to the active enzyme fails to give rise to the absorbance attributed to the flavin iminium ion. The detection of this spectroscopic signature only in the presence of the substrate provides further support for a covalent flavin intermediate during catalysis. Moreover, our crystallographic data are consistent with this observed substrate specificity; the glucose moiety is improperly oriented for participation in flavin-mediated covalent catalysis. STD-NMR experiments also indicate that there are differences between the UDP-Glc and the UDP-Gal*p* complexes. Although the uridine moieties of the nucleotide sugars bind similarly, the hexopyranose (Glc or Gal*p*) moieties do not. Indeed, the uridine-binding pocket exhibits excellent shape complementarity (Fig. 7a). In contrast, the region near the sugar moiety is more open to solvent, and cavities between the ligand and the enzyme are apparent. The excess space around the sugar residue is also consistent with the findings that UDP contributes a substantial portion of the substrate binding energy.[17,27]

The space around the sugar enabled the *in silico* reorientation of the Gal*p* moiety in the active site to generate the minimized model (Fig. 7b). With the exception of the potential hydrogen bond between the Gal*p* 6-OH and Arg280, the Gal*p* moiety in the minimized model does not make tight contacts with the protein, and empty cavities between the Gal*p* residue and protein are retained. These cavities allow space for molecular movement and are consistent with the chemical requirements for turnover. Specifically, UGM must be able to recognize both pyranose and furanose substrates and the galactose–flavin adduct. Thus, the data suggest that the UGM active site can accommodate all of these species.

Our model provides insight into how UGM can distinguish between related nucleotide sugars. This ability appears to be a physiological imperative. Estimates from other bacterial species place the cellular concentration of UDP-Glc in the low millimolar range, with the UDP-Gal*p* concentration generally believed to be significantly lower.[50–53] This level of competing UDP sugar could halt UDP-Gal*f* production if UGM is unable to discriminate against related UDP sugars. Our data show that the catalytically active form of UGM prefers to bind to UDP-Gal*p* over UDP-Glc. Moreover, our model suggests that UGM cannot place the sugar of UDP-Glc in the same orientation as that of UDP-Gal*p* because the equatorial C4-OH group of UDP-Glc would undergo a steric clash with the protein. This result explains why exposure of UDP-Glc to UGM fails to give rise to the spectroscopic signal indicative of the flavin iminium ion. Our model of the complex provides a solution to the apparent paradox of how UGM can discriminate between the two highly related structures UDP-Glc and UDP-Gal*p* yet turn over either UDP-Gal*p* or UDP-Gal*f*—two entities that are structurally very different.

In addition to providing insight into UGM catalysis, our structural studies can guide the identification of UGM inhibitors. The cavities of the UGM-binding pocket that allow substrate discrimination are locations to which small-molecule inhibitors[16–19] could bind. Knowledge of the function of conserved residues gained from this structure, along with an understanding of conformational changes upon binding, can facilitate the design of highly potent inhibitors. Such compounds may serve not only as valuable probes of cell wall biosynthesis in organisms such as *M. tuberculosis* but also as therapeutic leads.

Materials and Methods

Enzyme preparation

A previously described[20] pGEM-T Easy (Promega, Madison, WI) construct containing the UGM gene (*glf*) from *K. pneumoniae* was employed. The *glf* gene on this plasmid includes two alterations: the native C-terminal arginine was changed to a glycine codon and a C-terminal hexahistidine tag was encoded. The construct was transformed into BL21(DE3) *E. coli* cells (Novagen, Madison, WI). Terrific Broth supplemented with 200 mg/L ampicillin was inoculated with isolated transformants, and bacteria were incubated at 37 °C for 20 h without induction. Cells were harvested by centrifugation (10,000*g*) and resuspended in buffer containing 20 mM sodium phosphate (pH 7.4), 25 mM imidazole, and 300 mM NaCl. Cells were disrupted by treatment with lysozyme, ribonuclease A, 0.1% Triton X-100, and sonication (Branson 450 sonifier). Lysate was cleared by centrifugation (15,000*g*) and filtration (0.2 μM). Cleared lysate was purified by immobilized metal–ion affinity chromatography using a HisTrap HP column (GE Healthcare, Piscataway, NJ) on an AKTA FPLC system (Amersham Biosciences, Piscataway, NJ). UGM was eluted with a linear gradient of 0–500 mM imidazole in 50 mM sodium phosphate buffer (pH 7.4) with 300 mM sodium chloride. Typical yields were >30 mg/L, and pooled UGM fractions were >90% pure. Glycerol solutions (10% vol/vol) of UGM were vitrified in liquid nitrogen and stored at −80 °C.

K_d determination

Fluorescence polarization (FP) assays measuring ligand displacement by a UDP-fluorescein (UDP-Fl) probe were performed as described previously.[17] Purified UGM was thawed and dialyzed against 50 mM sodium phosphate (pH 7). Assays were conducted in a 384-well format in a final volume of 30 μL, with 15 nM UDP-Fl probe and 75 nM UGM. Concentrations of UDP (Sigma-Aldrich, St. Louis, MO), UDP-Gal*p* (Calbiochem, San Diego, CA), or UDP-Glc (Calbiochem) were varied from 0.5 μM for all ligands to 10 mM (UDP), 22 mM (UDP-Gal*p*), or 50 mM (UDP-Glc). Millipolarization values were measured using an Envision 2100 plate reader (Perkin-Elmer, Waltham, MA). Data were fitted, using Kaleidagraph software (Synergy Software USA), to $y=(a-d)/(1+(x/c)^{-b}+d)$, where a = maximum FP signal, b = slope, c = apparent K_d value, and d = minimum FP signal. K_d values were calculated from apparent K_d values using the equation $K_d = K_{d(app)}/(1+[UGM]/K_{d(UDP\text{-}Fl)})$, where $K_{d(UDP\text{-}Fl)}$ is the K_d value of UDP-Fl probe binding to UGM determined for the particular enzyme preparation (90 nM). The K_d value for UDP-Glc binding to reduced UGM was determined based on a decrease in FAD fluorescence using a QuantaMaster1 photon-counting fluorimeter (Photon Technology International, Birmingham, NJ), as described previously.[27]

UV/Vis spectroscopy and HPLC assay of UDP-Glc

Ligand titration profiles were performed similarly to previous methods[20] using a Cary 50 UV/Vis spectrophotometer (Varian, Palo Alto, CA). After the subtraction of buffer (50 mM sodium phosphate, pH 7) background absorbance, the absorbance of a solution containing 250 μM UGM, 20 mM sodium dithionite (Fluka, Steinheim, Germany), and phosphate buffer was measured using the scan mode (400–550 nm) before and after the addition of aliquots of 100 mM UDP-Gal*p* or UDP-Glc to generate titration curves.

UDP-Glc was tested as a potential substrate for UGM using an HPLC-based assay.[54] In this assay, substrate and product (typically UDP-Gal*p* and UDP-Gal*f*) are separated with an isocratic elution of 200 mM ammonium acetate (pH 8) on an anion-exchange column (CarboPac PA-100; Dionex, Sunnyvale, CA). UDP-Glc*p* was found to coelute with UDP-Gal*p*, and no additional peak (for the "product"

UDP-glucofuranose) was observed following incubation of reduced UGM with UDP-Glc*p*.

Crystallization of UGM

Prior to crystallization, UGM purified by immobilized metal–ion affinity chromatography was further purified by anion-exchange chromatography. UGM was dialyzed into 50 mM Hepes buffer (pH 7.0). Dialyzed samples were purified on a Mono Q 5/50 GL column (GE Healthcare) equilibrated with 50 mM Hepes (pH 7.0). UGM was eluted with a 0–30% linear gradient of 50 mM Hepes buffer (pH 7.0) and 1 M sodium chloride. Fractions containing UGM (identified by SDS-PAGE) were pooled and concentrated. Concentrated UGM was >99% pure, as assayed by SDS-PAGE. UGM was dialyzed into 20 mM Hepes buffer (pH 7.0) prior to crystallization.

All crystals were obtained using hanging-drop vapor diffusion,[55] with drops consisting of 1.5 μL of mother liquor and 1.5 μL of UGM (5 mg/mL). Sparse matrix screening using The Cryos Suite (Qiagen) was performed in the presence of 2 mM UDP-Glc, with each precipitant diluted by one-third by the addition of L-cysteine to a final concentration of 7 mM. L-Cysteine was previously identified as helpful for certain UGM crystallization conditions.[56] Initial conditions (Cryos condition no. 87) were optimized to give single yellow crystals that grew from clumps of crystalline precipitates over 1–2 weeks using a mother liquor of 85 mM ammonium acetate, 42 mM trisodium citrate (pH 5.6), 12.3% polyethylene glycol 4000, 7.5% glycerol, and 15 mM L-cysteine, with the protein solution containing 5 mM UDP-Glc. Crystals were vitrified in liquid N_2 after swiping through mother liquor supplemented with 0.9 M ammonium acetate and 2% glycerol.

Data were collected at the Advanced Photon Source (BioCARS, Argonne, IL). Phases were determined by molecular replacement using Phaser,[57] with the *K. pneumoniae* structure (PDB code 2BI8) as search model.[29] Refinement was performed using Refmac (v5.2.0019).[58] In the omit map of residue Arg174 in monomer A, electron density (3σ) can be seen to the δ-carbon (data not shown). The entire residue is modeled due to strong biochemical evidence indicating a role for the pyrophosphoryl group in binding.[30] In open monomer B, electron density (3σ) is seen to the β-carbon for Arg174. Figs. 3, 4, 6, and 7 were generated in PyMOL, and superposition (Fig. 3) was performed using that program's default algorithms.[59]

STD-NMR spectroscopy

STD-NMR was performed similarly to previous methods.[34] The final concentrations were 20 μM UGM (40 μM active sites), 4 mM ligand (UDP-Gal*p* or UDP-Glc), and 10 μM deuterated 2,2-dimethyl-2-silapentane-5-sulfonic acid in 50 mM K_2HPO_4/KH_2PO_4 (pH 7.6) in 99% D_2O. For reduced samples, concentrated sodium dithionite was added to a final concentration of 20 mM to otherwise identical samples under scrubbed argon gas. STD-NMR spectra were recorded on a DMX 750 with Cryoprobe (Bruker, Billerica, MA) at 300 K with 1024 scans. Continuous-wave saturation of protein resonances was performed at −1.0 ppm with a saturation time of 2 s. Phase cycling was used to subtract saturated spectra from reference spectra. A spin-lock pulse was found to provide a stable baseline and was used for all spectra. No STD signal was present in experiments performed in the absence of enzyme, indicating that saturation transfer from protein to ligand is the reason for the observed STD spectra. Ligand resonances were identified using previous assignments[34] and available databases (MMCD† and HMDB‡). Peak areas of STD spectra were measured using XWINNMR. STD values for UDP-Gal*p* were overall quite similar to those seen previously,[34] so we referenced our spectra in the same manner, with the largest STD peak (from protons 1′U/5U) set at 100% and with all other peak areas referenced to that value. The same assumptions regarding overlap were made for UDP-Gal*p* samples. The overlapping protons 3G and 6G(a) of UDP-Glc were assumed, for simplicity, to have equal STD values.

Energy-minimized active-site model

The UDP-Glc molecule of the oxidized UGM structure was modified to UDP-Gal*p* by inverting stereochemistry at C4. The β-phosphoryl and sugar moieties were rotated manually to position the carbon–β-phosphoryl oxygen bond in line with N5 of flavin. The UMP moiety was not moved. Energy minimization was performed on monomer A using Sybyl (Tripos, St. Louis, MO). Water molecules were removed, hydrogen atoms were added, and Gasteiger–Marsilli charges were calculated. Energy minimization used the Tripos force field and system defaults, using 100 rounds of minimization. The UDP-Gal*p* position was not fixed relative to the protein during minimization [e.g., the distance between the N5 position of flavin and the anomeric carbon (C1) was free to vary as minimization progressed].

Accession number

Coordinates and structure factors have been deposited in the PDB with accession number 3GF4.

Acknowledgements

This research was supported by a National Institutes of Health (NIH) grant (AI 063596 to L. L.K.). T.D.G. was supported by the NIH Biotechnology Training Program (GM08349). M.J.B. was funded by an NIH Molecular Biosciences Training Grant (GM07215) and a Steenbock Fellowship from the University of Wisconsin-Madison Department of Biochemistry. Use of the Advanced Photon Source was supported by the US Department of Energy, Basic Energy Sciences, Office of Science, under contract no. W-31-109-Eng-38. Use of the BioCARS Sector 14 was supported by the NIH National Center for Research Resources (RR 007707). NMR experiments were performed at the National Magnetic Resonance Facility at Madison, supported by NIH grants P41RR02301 (Biomedical Research Training Program/National Center for Research Resources) and P41GM66326 (National Institute of General Medical Sciences). This facility is also supported by the University of Wisconsin,

† mmcd.nmrfam.wisc.edu
‡ www.hmdb.ca

the NIH (RR02781 and RR08438), the National Science Foundation (DMB-8415048, OIA-9977486, and BIR-9214394), and the United States Department of Agriculture. We thank Dr. Kenneth Satyshur for data collection at BioCARS Beamline 14-ID-B, Dr. R. T. Raines for the use of fluorimeter equipment, and H. A. Steinberg for assistance with the figures.

Supplementary Data

Supplementary data associated with this article can be found, in the online version, at doi:10.1016/j.jmb.2009.05.081

References

1. Brennan, P. J. & Nikaido, H. (1995). The envelope of mycobacteria. *Annu. Rev. Biochem.* **64**, 29–63.
2. Jann, B., Shashkov, A. S., Kochanowski, H. & Jann, K. (1994). Structure of the O16 polysaccharide from *Escherichia coli* O16:K1: an NMR investigation. *Carbohydr. Res.* **264**, 305–311.
3. Nassau, P. M., Martin, S. L., Brown, R. E., Weston, A., Monsey, D., McNeil, M. R. & Duncan, K. (1996). Galactofuranose biosynthesis in *Escherichia coli* K-12: identification and cloning of UDP-galactopyranose mutase. *J. Bacteriol.* **178**, 1047–1052.
4. Köplin, R., Brisson, J. -R. & Whitfield, C. (1997). UDP-galactofuranose precursor required for formation of the lipopolysaccharide O antigen of *Klebsiella pneumoniae* serotype O1 is synthesized by the product of the $rfbD_{KPO1}$ gene. *J. Biol. Chem.* **272**, 4121–4128.
5. Stevenson, G., Neal, B., Liu, D., Hobbs, M., Packer, N. H., Batley, M. *et al.* (1994). Structure of the O antigen of *Escherichia coli* K-12 and the sequence of its *rfb* gene cluster. *J. Bacteriol.* **176**, 4144–4156.
6. Raetz, C. R. & Whitfield, C. (2002). Lipopolysaccharide endotoxins. *Annu. Rev. Biochem.* **71**, 635–700.
7. Latge, J. P., Kobayashi, H., Debeaupuis, J. P., Diaquin, M., Sarfati, J., Wieruszeski, J. M. *et al.* (1994). Chemical and immunological characterization of the extracellular galactomannan of *Aspergillus fumigatus*. *Infect. Immun.* **62**, 5424–5433.
8. McConville, M. J., Homans, S. W., Thomas-Oates, J. E., Dell, A. & Bacic, A. (1990). Structures of the glycoinositolphospholidpids from *Leishmania major*. A family of novel galactofuranose-containing glycolipids. *J. Biol. Chem.* **265**, 7385–7394.
9. Previato, J. O., Gorin, P. A., Mazurek, M., Xavier, M. T., Fournet, B., Wieruszeski, J. M. & Mendonca-Previato, L. (1990). Primary structure of the oligosaccharide chain of lipopeptidophosphoglycan of epimastigote forms of *Trypanosoma cruzi*. *J. Biol. Chem.* **265**, 2518.
10. Pan, F., Jackson, M., Ma, Y. F. & McNeil, M. R. (2001). Cell wall core galactofuran synthesis is essential for growth of mycobacteria. *J. Bacteriol.* **183**, 3991–3998.
11. El-Ganiny, A. M., Sanders, D. A. & Kaminskyj, S. G. (2008). *Aspergillus nidulans* UDP-galactopyranose mutase, encoded by ugmA plays key roles in colony growth, hyphal morphogenesis, and conidiation. *Fungal Genet. Biol.* **45**, 1533–1542.
12. Damveld, R. A., Franken, A., Arentshorst, M., Punt, P. J., Klis, F. M., van den Hondel, C. A. & Ram, A. F. (2008). A novel screening method for cell wall mutants in *Aspergillus niger* identifies UDP-galactopyranose mutase as an important protein in fungal cell wall biosynthesis. *Genetics*, **178**, 873–881.
13. Schmalhorst, P. S., Krappmann, S., Vervecken, W., Rohde, M., Muller, M., Braus, G. H. *et al.* (2008). Contribution of galactofuranose to the virulence of the opportunistic pathogen *Aspergillus fumigatus*. *Eukaryotic Cell*, **7**, 1268–1277.
14. Kleczka, B., Lamerz, A.-C., van Zandbergen, G., Wenzel, A., Gerardy-Schahn, R., Wiese, M. & Routier, F. H. (2007). Targeted gene deletion of *Leishmania major* UDP-galactopyranose mutase leads to attenuated virulence. *J. Biol. Chem.* **282**, 10498–10505.
15. Pederson, L. L. & Turco, S. J. (2003). Galactofuranose metabolism: a potential target for antimicrobial chemotherapy. *Cell. Mol. Life Sci.* **60**, 259–266.
16. Scherman, M. S., Winans, K. A., Stern, R. J., Jones, V., Bertozzi, C. R. & McNeil, M. R. (2003). Drug targeting *Mycobacterium tuberculosis* cell wall synthesis: development of a microtiter plate-based screen for UDP-galactopyranose mutase and identification of an inhibitor from a uridine-based library. *Antimicrob. Agents Chemother.* **47**, 378–382.
17. Soltero-Higgin, M., Carlson, E. E., Phillips, J. H. & Kiessling, L. L. (2004). Identification of inhibitors for UDP-galactopyranose mutase. *J. Am. Chem. Soc.* **126**, 10532–10533.
18. Carlson, E. E., May, J. F. & Kiessling, L. L. (2006). Chemical probes of UDP-galactopyranose mutase. *Chem. Biol.* **13**, 825–837.
19. Dykhuizen, E. C., May, J. F., Tongpenyai, A. & Kiessling, L. L. (2008). Inhibitors of UDP-galactopyranose mutase thwart mycobacterial growth. *J. Am. Chem. Soc.* **130**, 6706–6707.
20. Soltero-Higgin, M., Carlson, E. E., Gruber, T. D. & Kiessling, L. L. (2004). A unique catalytic mechanism for UDP-galactopyranose mutase. *Nat. Struct. Mol. Biol.* **11**, 539–543.
21. Fullerton, S. W. B., Daff, S., Sanders, D. A. R., Ingledew, W. J., Whitfield, C., Chapman, S. K. & Naismith, J. H. (2003). Potentiometric analysis of UDP-galactopyranose mutase: stabilization of the flavosemiquinone by substrate. *Biochemistry*, **42**, 2104–2109.
22. Sanders, D. A. R., Staines, A. G., McMahon, S. A., McNeil, M. R., Whitfield, C. & Naismith, J. H. (2001). UDP-galactopyranose mutase has a novel structure and mechanism. *Nat. Struct. Biol.* **8**, 858–863.
23. Barlow, J. N., Girvin, M. E. & Blanchard, J. S. (1999). Positional isotope exchange catalyzed by UDP-galactopyranose mutase. *J. Am. Chem. Soc.* **121**, 6968–6969.
24. Zhang, Q. & Liu, H.-W. (2001). Mechanistic investigation of UDP-galactopyranose mutase from *Escherichia coli* using 2- and 3-fluorinated UDP-galactofuranose as probes. *J. Am. Chem. Soc.* **123**, 6756–6766.
25. Soltero, M. L., Carlson, E. E. & Kiessling, L. L. (2003). A proposal for the catalytic mechanism of UDP-galactopyranose mutase. University of Wisconsin-Madison, Madison, WI.
26. Huang, Z., Zhang, Q. & Liu, H.-W. (2003). Reconstitution of UDP-galactopyranose mutase with 1-deaza-FAD and 5-deaza-FAD: analysis and mechanistic implications. *Bioorg. Chem.* **31**, 494–592.
27. Itoh, K., Huang, Z. & Liu, H. w. (2007). Synthesis and analysis of substrate analogues for UDP-galactopyranose mutase: implication for an oxocarbenium ion intermediate in the catalytic mechanism. *Org. Lett.* **9**, 879–882.

28. Miller, S. M. (2004). A new role for an old cofactor. *Nat. Struct. Mol. Biol.* **11**, 497–498.
29. Beis, K., Srikannathasan, V., Liu, H., Fullerton, S. W. B., Bamford, V. A., Sanders, D. A. R. *et al.* (2005). Crystal structures of *Mycobacterium tuberculosis* and *Klebsiella pneumoniae* UDP-galactopyranose mutase in the oxidised state and *Klebsiella pneumoniae* UDP-galactopyranose mutase in the (active) reduced state. *J. Mol. Biol.* **348**, 971–982.
30. Chad, J. M., Sarathy, K. P., Gruber, T. D., Addala, E., Kiessling, L. L. & Sanders, D. A. R. (2007). Site-directed mutagenesis of UDP-galactopyranose mutase reveals a critical role for the active-site, conserved arginine residues. *Biochemistry*, **46**, 6723–6732.
31. Yuan, Y., Bleile, D. W., Wen, X., Sanders, D. A. R., Itoh, K., Liu, H.-W. & Pinto, B. M. (2008). Investigation of binding of UDP-Gal*f* and UDP-[3-F]Gal*f* to UDP-galactopyranose mutase by STD-NMR spectroscopy, molecular dynamics, and CORCEMA-ST calculations. *J. Am. Chem. Soc.* **130**, 3157–3168.
32. Yao, X., Bleile, D. W., Yuan, Y., Chao, J., Sarathy, K. P., Sanders, D. A. *et al.* (2008). Substrate directs enzyme dynamics by bridging distal sites: UDP-galactopyranose mutase. *Proteins*, **74**, 972–979.
33. Williams, R. F. & Bruice, T. C. (1976). The kinetics and mechanisms of 1,5-dihydroflavin reduction of carbonyl compounds and flavin oxidation of alcohols: 2. Ethyl pyruvate, pyruvamide, and pyruvic acid. *J. Am. Chem. Soc.* **98**, 7752–7768.
34. Yuan, Y., Wen, X., Sanders, D. A. R. & Pinto, B. M. (2005). Exploring the mechanism of binding of UDP-galactopyranose to UDP-galactopyranose mutase by STD-NMR spectroscopy and molecular modeling. *Biochemistry*, **44**, 14080–14089.
35. Angyal, S. J. & Pickles, V. A. (1972). Equilibria between pyranoses and furanoses. *Aust. J. Chem.* **25**, 1695–1710.
36. Davis, I. W., Leaver-Fay, A., Chen, V. B., Block, J. N., Kapral, G. J., Wang, X. *et al.* (2007). MolProbity: all-atom contacts and structure validation for proteins and nucleic acids. *Nucleic Acids Res.* **35**, W375–W383.
37. Mayer, M. & Meyer, B. (1999). Characterization of ligand binding by saturation transfer difference NMR spectroscopy. *Angew. Chem. Int. Ed. Engl.* **38**, 1784–1788.
38. Eppe, G., Peltier, P., Daniellou, R., Nugier-Chauvin, C., Ferrières, V. & Vincent, S. P. (2009). Probing UDP-galactopyranose mutase binding pocket: a dramatic effect on substitution of the 6-position of UDP-galactofuranose. *Bioorg. Med. Chem. Lett.* **19**, 814–816.
39. Errey, J., Mann, M., Fairhurst, S., Hill, L., McNeil, M. R., Naismith, J. *et al.* (2009). Sugar nucleotide recognition by *Klebsiella pneumoniae* UDP-D-galactopyranose mutase: fluorinated substrates, kinetics and equilibria. *Org. Biomol. Chem.* **7**, 1009.
40. Rutledge, L. R., Campbell-Verduyn, L. S., Hunter, K. C. & Wetmore, S. D. (2006). Characterization of nucleobase–amino acid stacking interactions utilized by a DNA repair enzyme. *J. Phys. Chem. B*, **110**, 19652–19663.
41. Ellis, J. J., Broom, M. & Jones, S. (2007). Protein–RNA interactions: structural analysis and functional classes. *Proteins*, **66**, 903–911.
42. Zacharias, N. & Dougherty, D. A. (2002). Cation–pi interactions in ligand recognition and catalysis. *Trends Pharmacol. Sci.* **23**, 281–287.
43. Vyas, N. K., Vyas, M. N. & Quiocho, F. A. (1988). Sugar and signal-transducer binding sites of the *Escherichia coli* galactose chemoreceptor protein. *Science*, **242**, 1290–1295.
44. Hashimoto, H. (2006). Recent structural studies of carbohydrate-binding modules. *Cell. Mol. Life Sci.* **63**, 2954–2967.
45. Borrok, M. J., Kiessling, L. L. & Forest, K. T. (2007). Conformational changes of glucose/galactose-binding protein illuminated by open, unliganded, and ultra-high-resolution ligand-bound structures. *Protein Sci.* **16**, 1032–1041.
46. Beverley, S. M., Owens, K. L., Showalter, M., Griffith, C. L., Doering, T. L., Jones, V. C. & McNeil, M. R. (2005). Eukaryotic UDP-galactopyranose mutase (GLF gene) in microbial and metazoal pathogens. *Eukaryotic Cell*, **4**, 1147–1154.
47. Bakker, H., Kleczka, B., Gerardy-Schahn, R. & Routier, F. (2005). Identification and partial characterization of two eukaryotic UDP-galactopyranose mutases. *Biol. Chem.* **386**, 657–661.
48. Koellner, G., Bzowska, A., Wielgus-Kutrowska, B., Luić, M., Steiner, T., Saenger, W. & Stepiński, J. (2002). Open and closed conformation of the *E. coli* purine nucleoside phosphorylase active center and implications for the catalytic mechanism. *J. Mol. Biol.* **315**, 351–371.
49. Morris, V. K. & Izard, T. (2004). Substrate-induced asymmetry and channel closure revealed by the apoenzyme structure of *Mycobacterium tuberculosis* phosphopantetheine adenylyltransferase. *Protein Sci.* **13**, 2547–2552.
50. Tweeddale, H., Notley-McRobb, L. & Ferenci, T. (1998). Effect of slow growth on metabolism of *Escherichia coli*, as revealed by global metabolite pool ("metabolome") analysis. *J. Bacteriol.* **180**, 5109–5116.
51. Buckstein, M. H., He, J. & Rubin, H. (2008). Characterization of nucleotide pools as a function of physiological state in *Escherichia coli*. *J. Bacteriol.* **190**, 718–726.
52. Bochner, B. R. & Ames, B. N. (1982). Complete analysis of cellular nucleotides by two-dimensional thin layer chromatography. *J. Biol. Chem.* **257**, 9759–9769.
53. Ramos, A., Boels, I. C., de Vos, W. M. & Santos, H. (2001). Relationship between glycolysis and exopolysaccharide biosynthesis in *Lactococcus lactis*. *Appl. Environ. Microbiol.* **67**, 33–41.
54. Lee, R., Monsey, D., Weston, A., Duncan, K., Rithner, C. & McNeil, M. R. (1996). Enzymatic synthesis of UDP-galactofuranose and an assay for UDP-galactopyranose mutase based on high-performance liquid chromatography. *Anal. Biochem.* **242**, 1–7.
55. McPherson, A. (1982). *Preparation and Analysis of Protein Crystals.* John Wiley & Sons, Inc., New York.
56. Sanders, D. A. R., McMahon, S. A., Leonard, G. L. & Naismith, J. H. (2001). Molecular placement of experimental electron density: a case study on UDP-galactopyranose mutase. *Acta Crystallogr. Sect. D*, **57**, 1415–1420.
57. Storoni, L. C., McCoy, A. J. & Read, R. J. (2004). Likelihood-enhanced fast rotation functions. *Acta Crystallogr. Sect. D*, **60**, 432–438.
58. Murshudov, G. N., Vagin, A. A. & Dodson, E. J. (1997). Refinement of macromolecular structures by the maximum-likelihood method. *Acta Crystallogr. Sect. D*, **53** , 240–255.
59. Delano, W. L. (2002). *The PyMOL Molecular Graphics System.* Delano Scientific, Palo Alto, CA, USA.